Model-based Optimization of Lead Configurations in Deep Brain Stimulation

Ruben Cubo

Department of Information Technology
Uppsala University
Email: ruben.cubo@it.uu.se

Mattias Åström

Department of Biomedical Engineering
Linköping University
Email: matas@imt.liu.se

Alexander Medvedev

Department of Information Technology
Uppsala University
Email: am@it.uu.se

Abstract—**Deep Brain Stimulation (DBS) is an established treatment in Parkinson's Disease whose underlying biological mechanisms are however unknown. Mathematical models aiming at a better understanding of how DBS works through the stimulation of the electrical field inside the brain tissue have been developed in the past years. This study deals with** *in silico* **optimization of the stimuli delivered to the brain using actual clinical data and a Finite Element Method (FEM) approach. The goal is to cover a given target volume and limit the spread of the stimulation beyond it to avoid possible side effects. The fraction of the volume of activated tissue within the target and the fraction of the stimulation field that spreads beyond it are computed in order to quantify the performance of the stimuli configuration. First, a state-of-the-art lead is considered, in both single active contact and multiple active contact stimulation scenarios. A comparison with a field-steering lead is further presented. The obtained results demonstrate feasibility of multiple contact stimulation through better shaping the stimuli and effectively using field steering.**

Keywords–Deep Brain Stimulation; Optimization; Convex optimization; Field Steering; Parkinson Disease

I. INTRODUCTION

Deep Brain Stimulation (DBS) is a neurosurgical procedure that consists of delivering electrical stimuli, usually rectangular biphasic pulses, to a target inside the brain by using one or several surgically implanted leads. The goal of the therapy is the alleviation of symptoms of various neurological diseases, such as Parkinson's Disease (PD) [1], epilepsy [2], dystonia [3], and others. DBS mostly replaced surgical lesioning and ablation procedures because of its reversibility, flexibility, and individualization potential [4]. The interest in DBS has spread to other areas of medicine, e.g. psychiatry, with applications in diseases such as schizophrenia [5] or Tourette Syndrome [6]. In the case of PD, since the surgery of DBS is quite complicated and costly compared to treatment with drugs, physicians usually choose advanced patients for this procedure when pharmacotherapy, in particular with levodopa, has lost effectiveness or has severe side effects [1]. Although some studies suggest that an earlier implantation could be beneficial [7].

The principle of DBS is in delivering mild electrical pulses via a chronically implanted lead, whose active contacts are in the subcortical area, where a target area is defined. Prior to the operation, patients undergo clinical examination by a multidisciplinary team, as well as medical imaging. Based on the images, the physician pinpoints a target area, which is in PD usually located in the basal ganglia area of the brain, with the subthalamic nucleus (STN) being of particular

interest. A few weeks after the surgery, the patients undergo a lengthy trial-and-error programming period to tune the stimuli delivered to the brain.

The physiological mechanism of DBS and its long-term effects on the brain still remain unknown, and the therapeutical outcome is difficult to predict. Furthermore, because of uncertainties in the position of the leads or improperly tuned stimulation settings, the stimulated volume might go beyond the target causing undesirable side effects [8]. Shaping the stimuli so that the stimulated volume covers the intended target and does not spill outside of it is thus important for maximization of the therapeutical benefits and minimization of the side effects.
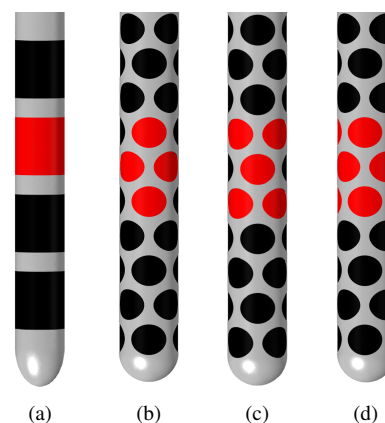

Figure 1. Lead configurations for the conventional lead (a), field-steering Diamond-4 (b), X-5 (c) and X-8 (d). Active contacts are marked in red.

Currently used lead designs, mostly from Medtronics (see Figure 1(a)), were originally adapted from cardiac pacing technology and have not evolved much since then. Meanwhile, the insights into neurostimulation and field steering obtained in recent years through Finite Element Method (FEM) based multiphysics simulation and neuron models, along with the exponential improvement of computational capabilities, open up for more sophisticated and individualized solutions, aiming to shorten the programming time and to better understand the underlying mechanisms [9].

Addressing the shortcomings of the currently used designs, novel leads have been developed by companies, such as 3Win (Belgium), Sapiens (The Netherlands) or Aleva (Switzerland), which could be configured in more versatile spacial settings, taking advantage of field steering techniques to tune the

stimuli. As seen in the contacts of the leads shown in Figure 1, while the conventional state-of-the-art lead delivers a radially symmetric stimulation over the whole cylindrical contact, the field steering one is capable of asymmetrical stimulation that can be tailored to the target area anatomy [10].

A possibility for performance improvement in the existing state-of-the-art electrodes is offered by a multicontact approach, i.e. manipulating the stimuli simultaneously using two or more active contacts. It has the benefit of allowing further shaping of the activated tissue area and thus providing more flexibility.

This manuscript is composed as follows. In Section 2, an overview of the FEM mathematical model is given, along with different neuronal stimulation quantification schemes. Afterwards, the optimization technique used is presented. In Section 3, the results of the optimized stimuli are outlined, for a single active contact, for multiple active contacts, and using field steering lead configurations. Conclusions, limitations, and future work are discussed in Section 4.

II. Models and Methods

A. Electric Field Model

The first step to compute optimized stimuli is to obtain the electric field distribution for a given electrode geometry. The electric potential is obtained by solving the equation of steady currents in the tissue:

$$\nabla \cdot (\sigma \nabla u) = 0, \tag{1}$$

where u is the electric potential, σ the electric conductivity, and ∇ is gradient. The electric field $\mathbf{E}$ is obtained by taking the negative gradient of u:

$$\mathbf{E} = -\nabla u. \tag{2}$$

Model (1) can be solved numerically using a FEM solver. The model geometry considered in this study consists of the bulk brain tissue, the lead, and an encapsulation layer surrounding it.

The bulk tissue is represented as a cube with a side of 0.4 m centered on the tip of the lead that is grounded on the outer surfaces to simulate the ground in the implanted pulse generator. Although the brain tissue is heterogeneous and anisotropic in reality, these effects are beyond the scope of this paper, see [9][11] for details. Although the brain tissue has several components, e.g., white matter, gray matter, cerebrospinal fluid and blood vessels, its conductivity can be approximated as homogeneous with $\sigma = 0.1\ S/m$ [12].

Two lead designs were considered for this study: a widely used state-of-the-art lead and a field steering lead. The former has cylindrical contacts with a height of 1.5 mm and a separation between contacts of 0.5 mm. The latter has elliptical contacts. To facilitate field steering, the rows are rotated 45 degrees to each other with respect to the lead axis, as shown in Figures 1(b),1(c), and 1(d). Both leads have a diameter of 1.27 mm.

An encapsulation layer is formed around a lead implanted in the brain due to the reaction of the body to a foreign object [13]. Its thickness and conductivity are still open to debate and

might be patient specific. Following [9], a 0.5 mm thick layer with a conductivity of 0.18 S/m is considered.

The stimulation is modeled as a boundary condition at the active contacts surface while the non-active contacts are left floating. It should be noted that model (1) is a linear partial differential equation, and thus, it is enough to compute the field distribution for a unit stimulus and then scale it accordingly, which transformation will simplify the computations.

The model has been implemented in COMSOL 4.3b (Comsol AB, Sweden). The solutions obtained by the FEM solver were then equidistantly gridded on a $70 \times 70 \times 60$ grid centered at the lead tip and expanding 16 mm in the axes perpendicular to the lead and 20 mm in the lead axis, in order to be exported for further processing.

Several field distributions were computed:

- State-of-the-art lead: Distributions with one active contact and the rest floating were computed at first. In addition to that, field distributions with the grounded inactive contacts were computed. This was done to enable summing up them for the multicontact approach, since the effect of one active contact on the others when left floating can be computed.

- Field steering lead: Distributions for the different configurations considered (Diamond-4, X-5, X-8, shown in Figure 1) were computed for each row of contacts.

B. Quantification of activated volumes

Volumes of activated tissue can be quantified by using axon models under the methodology by McNeal [14]. While axon models yield precise results, the procedure is computationally expensive and the neuron network must be known to some degree. Other approaches involve functions that approximate the activated volume without taking into account the anatomy of the neurons, such as Rattay's activation function [15] or the electric field. These have the advantage of requiring less computations and only a stationary analysis. However, using second derivatives might result in numerical issues, in particular in the area near the lead. Furthermore, it was shown that the electric field provides more robust means for quantifying neuronal stimulation [16]. Thus, for this study, the electric field will be used. The activated neurons are distinguished from the rest by applying a threshold value to the electric field that will depend on the neuron anatomy and the characteristics of the pulse itself [16].

To place the pre-computed by the FEM solver electric field at the proper position, conventional translation-rotation algebra is utilized. Assuming that the tip of the lead is at the origin, the set of operations is given by:

$$\mathbf{E}_{\text{eval}} = R_{\text{rot}}R_{\text{z}}\mathbf{E} + \mathbf{x}_{\text{lead}}, \tag{3}$$

where $\mathbf{E}$ and $\mathbf{E}_{\text{eval}}$ are the original and positioned electric field vectors respectively, R_{rot} is a rotation matrix which aligns the field with the given lead vector, R_z is a rotation matrix with respect to the Z axis (used for field steering), and $\mathbf{x}_{\text{lead}}$ is the lead position.

Once the field is properly positioned and filtered with the aforementioned threshold, intersection volumes are computed under a methodology similar to [17]. Two of them are of particular interest: the activated volume of the target area and

the activated volume outside the target area. The topology of the target area is taken from an atlas of potential regions for therapeutical stimulation and can be assumed to be convex. Whether the electric field points are inside of the convex hull of the target area or not is checked with an additional function [18].

C. Optimization scheme

In order to optimize the stimuli, the following optimization problem can be defined:

$$\min_{u_i} J(u_i), \qquad (4)$$

where u_i are the optimization variables (in this case, the electric potential or potentials of the stimuli) and $J(u_i)$ is a cost function to be defined (ideally, a convex function).

The following cost function is proposed:

$$\begin{aligned} J(u_i) &= p_{\text{Spill}}(u_i) \left(\frac{100 - p_{\text{Act}}(u_i)}{100 - p_{\text{Th}}} \right) & p_{\text{Act}} \le p_{\text{Th}} \\ J(u_i) &= p_{\text{Spill}}(u_i) & p_{\text{Act}} > p_{\text{Th}} \end{aligned} \qquad (5)$$

where p_{Spill} is the fraction of the activated volume that lies outside the target, p_{Act} is the fraction of the target which is activated and p_{Th} is the minimum activation required of the target. All of them are given in percent for illustration. For this study, p_{Th} is set at 95%.

The motivation behind the cost function above is that it is continuous and convex, since both p_{Act} and p_{Spill} are monotonically nondecreasing with the amplitude of the stimulus. An example of cost function (5) dependence on the stimuli amplitude can be seen in Figure 2.
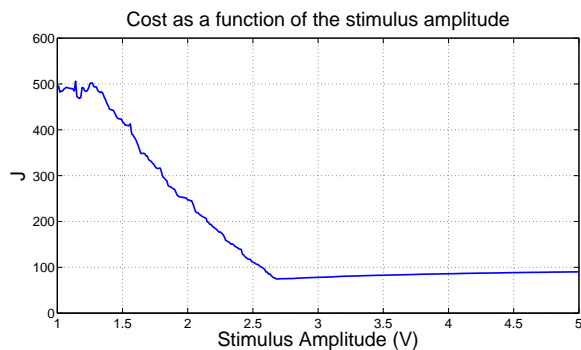

Figure 2. Example of cost function J as a function of the stimulus amplitude

The small peaks that appear in Figure 2 occur because of issues with the volume computation. They arise since the geometry used for both the activation volume and the target is defined in convex hulls of a discrete cloud of points. Although this makes the function non-convex in practice, the peaks are small enough to be skipped by increasing the step size of the optimization algorithm. A minimum step size of 0.002 V was taken.

III. RESULTS

A. Single Contact

To optimize stimulation with only one active contact, two approaches can be considered. First, the contact can be fixed and only the stimulus amplitude is optimized. Second, the

active contact is left as an additional optimization variable, restricted to taking a single value in the set $C_s = \{0, 1, 2, 3\}$, where contact 0 is the most distal and 3 is the most proximal. Due to the possibility of choosing the active contact at will and to illustrate the efficiency of the optimization method, the second approach is selected in this study.

The free contact approach will divide the optimization into four problems with fixed contacts. In order to speed up the computations, best active contact could be chosen without optimization. By examining $J(u_i)$ given by (5), it can be easily seen that as long as there is an intersection between the activated volume and the target for at least one of the contacts, the cost function will be lower in general for the optimal contact no matter how big u_i is. So, it is enough to do a single evaluation of the cost function for a given value of u_i to choose the contact. Said value cannot be too low, since it might yield empty intersections, or too high since it will take too much time to calculate due to the number of points involved. Thus, the evaluation is performed with low u_i and then if the intersection is empty, u_i is set to a higher value.

Optimization was performed for 65 lead positions whose clinical data stated a single contact stimulation with an activation threshold of 175 and 200 V/m for comparison. Comparing the results with respect to the clinical settings is of great interest, so the fraction of configurations estimated successfully by the optimization algorithm with respect to the clinical settings was computed as well.
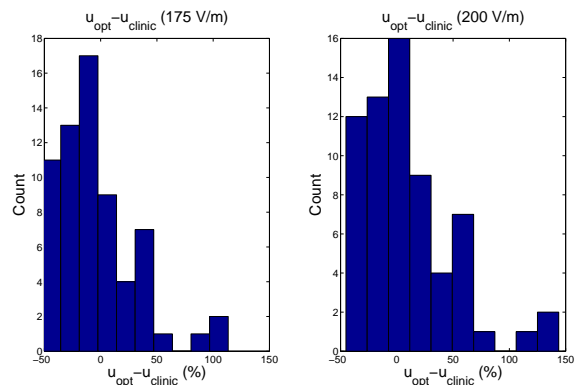

Figure 3. Discrepancy of amplitude for 175 and 200 V/m

TABLE I. SINGLE CONTACT OPTIMIZATION

Threshold: 200 V/m	
Correct contact (%):	53.8
1 contact error (%):	35.4
Discrepancy of amplitude (%):	9 ± 41
Threshold: 175 V/m	
Correct contact (%):	50.7
1 contact error (%):	38.4
Discrepancy of amplitude (%):	-4 ± 35

It can be seen from Table I that the mathematical model and the defined target predict the clinically used contact in roughly a half of the cases. In addition, in almost all of the cases, the predicted optimal contact is an immediate neighbor of the one specified in the clinical data. In some cases, there is no significant difference in the values of the cost function, so either contact can be utilized, according to the calculated

values. In addition, the predicted optimized stimuli amplitude is fairly close to the clinical one (see Figure 3, which suggest that in most cases a threshold between 175 and 200 V/m might be sufficient. It comes though with a high standard deviation.

B. Multiple Contacts

Another approach would be to allow for multiple active contact configurations. To simplify the field modeling, the linearity of (1) is exploited. In particular, the field distribution for each contact stimulating with an unit stimulus while the others are grounded is computed first, denoting it as $\mathbf{E}_{0,i}$ for the i-th contact. Then the relation between active contacts and the rest in floating configuration is computed. It follows a linear relationship and is denoted as α_{ki}, which would represent the effect the i-th contact has over the k-th contact when the k-th contact is floating. This is used to transform from an active-grounded to an active-floating configuration, when the contributions are being summed.

The electric field distributions result from a sum of four contacts, with the stimuli given by the active contacts, denoted by u_i and representing the degrees of freedom and the non-active (floating) contacts contributing with the terms characterized by the corresponding α_{ki}. For example, for a 2-contact scheme, one gets

$$\mathbf{E}_{2cont}(\mathbf{r}) = u_1\mathbf{E}_{0,1} + u_2\mathbf{E}_{0,2} + \\ + (u_1\alpha_{31} + u_2\alpha_{32})\mathbf{E}_{0,3} + (u_1\alpha_{41} + u_2\alpha_{42})\mathbf{E}_{0,4} \quad (6)$$

It should be noted that the numbering of the contacts above was arbitrary, and it could be any combination of them.
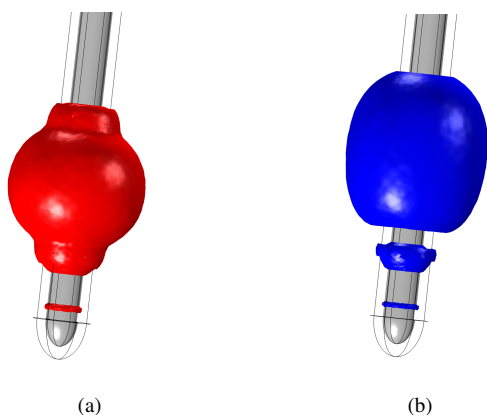

(a)　　　　　　　　(b)

Figure 4. Isolevels for $E = 200\ V/m$ for a single active contact (a) and two active contacts (b)

As can be seen in Figure 4(b), multiple active contacts might be useful to tailor the stimulation so that it achieves a similar activated volume with less overspill. The results is in principle dependent on the position of the target with respect to the active contact in the single contact approach. If the target is located next to the active contact, then it would be probably more useful to consider just a single contact stimulation. However, if the target is located in between two contacts, shaping the stimulation with these two contacts might be beneficial.

The optimization method is similar to the one described in the previous section for a single contact. To speed up computations, only the configurations which involve neighbouring
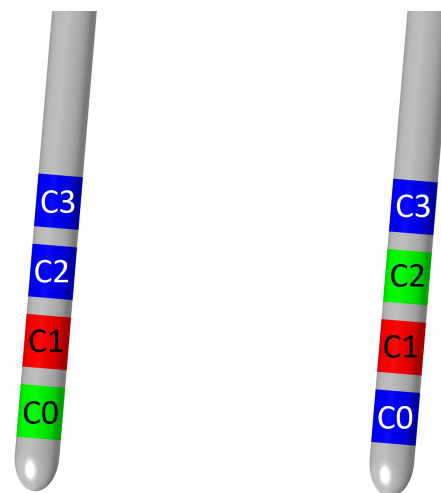

Figure 5. Example of considered multicontact configurations, with Contact 1 as the optimal (in red) and Contacts 0 (left) and 2 (right) as secondary (in green)

contacts to the ones obtained in the single contact approach are considered. So, for example, if the optimal contact is contact 1, only combinations which involve contacts 1 and 0 and 1 and 2 are considered (see Figure 5).
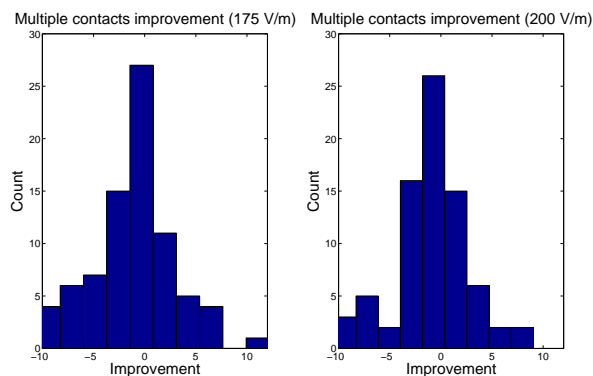

Figure 6. Improvement of overspill for 175 and 200 V/m for the multicontact approach

TABLE II. MULTIPLE CONTACT OPTIMIZATION

Threshold: 200 V/m	
Improvement cases (%):	38.7
Overspill improvement (percentage points):	2.00 ± 2.28
Threshold: 175 V/m	
Improvement cases (%):	37.5
Overspill improvement (percentage points):	2.67 ± 2.83

Results are summarized in Figure 6 and Table II. The improvement is, as expected, situational, and appears only in a part of the cases. However, the improvement can be significant, with a decrease of up to 5 or 6 percentage points in the absolute value of the overspill with respect to the single contact approach. It should be noted that the state-of-the-art lead considered here features a small distance between contacts. Better results could be achieved for larger distances between

contacts, since it is more likely that the target lies between contacts.

C. Field Steering

As was investigated in [17][19], field steering yields better results regarding overspill than with the state-of-the-art radial stimulation. In this study, the optimization scheme described above was implemented to obtain the optimal stimulus amplitude.

Three different configurations were tested, as illustrated in Figure 1. The parameters to optimize would be, for each configuration, the rows where the active contacts are located and the orientation of the lead with respect to its axis. To speed up computations, the optimization followed a similar scheme to the one with multiple contacts, taking as a baseline the results obtained with single contacts and state-of-the-art lead. Due to different shapes of the contacts, the rows at roughly the same height are considered, plus their neighbors.
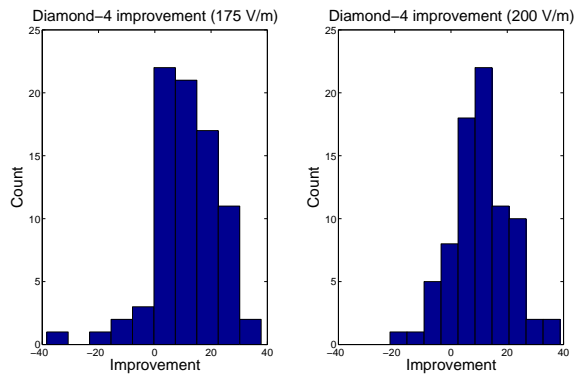

Figure 7. Improvement distribution using the Diamond 4 configuration

TABLE III. DIAMOND 4 CONFIGURATION IMPROVEMENT

Threshold: 200 V/m	
Improvement cases (%):	87.5
Overspill improvement (percentage points):	10.37 ± 10.52
Threshold: 175 V/m	
Improvement cases (%):	91.25
Overspill improvement (percentage points):	11.48 ± 11.63

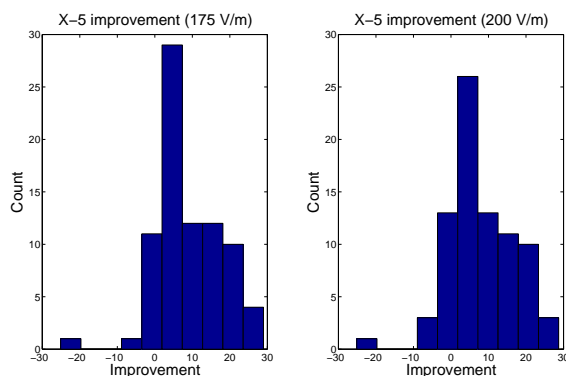Figure 8. Improvement distribution using the X-5 configuration

Table IV. X-5 configuration improvement

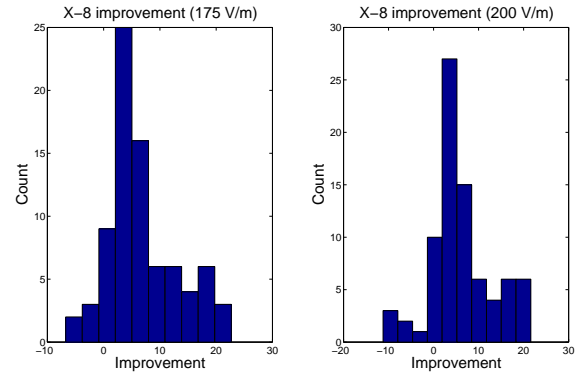| Threshold: 200 V/m	
Improvement cases (%):	88.75
Overspill improvement (percentage points):	8.65 ± 10.67
Threshold: 175 V/m	
Improvement cases (%):	92.5
Overspill improvement (percentage points):	9.76 ± 10.37

Figure 9. Improvement distribution using the X-8 configuration

Results are summarized in Figures 7 - 9 and Tables III - V. In almost all cases, there is an improvement in the overspill with respect to the one-contact approach. The improvement is largest in average with the Diamond-4 configuration (see Figure 7). The high standard deviation comes from the variety of geometries considered, making the improvement heavily dependent on the lead position with respect of the target. Some cases were observed where the X-5 or X-8 configurations achieved better results that could be because of the lead location.

IV. DISCUSSION

Using optimization schemes in order to scale the stimulus amplitude of the active contact or contacts could yield an activation volume that better covers a given target, limiting, at the same time, as much as possible stimulation beyond the target. This study compares the state-of-the-art one-contact approach with a multiple contact approach and field steering.

In the analysis of the one-contact approach, it was seen that selecting the active contact freely for a given target, a simple model predicts the clinically used contact in roughly a half of the times in the considered lead population. Furthermore, in some cases, there is no significant difference between the scores of the clinical and the optimal configurations.

In the multicontact approach, allowing for multiple contacts improved the overspill in around 38% of the cases. It must be noted that the effect is limited by the small distance

Table V. X-8 configuration improvement

Threshold: 200 V/m	
Improvement cases (%):	90
Overspill improvement (percentage points):	11.51 ± 10.63
Threshold: 175 V/m	
Improvement cases (%):	91.25
Overspill improvement (percentage points):	11.56 ± 10.41

between the contacts and could be more significant for a larger separation of the contacts.

Finally, the results obtained are compared to field steering configurations. A significant improvement of the overspill with a decrease of 10 percentage points in average was found in all cases, with an average decrease of 18 percentage points for the Diamond 4 configuration.

However, the results obtained in this study are valid under some limitations. First, the brain tissue was assumed to be homogeneous, when this is not the case and significant (patient specific) differences may arise [9]. Furthermore, the encapsulation layer surrounding the lead has uncertain physical properties, such as the conductivity and the thickness, both of which might be time variant [20]. In addition, considering the electric field as a predictor of whether a neuron is stimulated or not is an approximation. A more thorough analysis would need a complete neuron population model. Finally, the results obtained assume a certain target structure, which may be patient specific as well. Results should be verified against therapeutic outcomes, but the latter are not yet available for this study.

Despite the mentioned limitations, this study highlights how using optimization schemes and geometric arguments can help to choose optimal stimuli and facilitate the comparison between different configurations. Further work could add more optimization schemes, such as using electric field differences between a target electric field distribution and the one given by the lead instead of geometry. In addition, it would be worthwhile to study the influence of the encapsulation tissue properties and the anisotropies of the brain tissue.

References

[1] J. A. Obeso, C. W. Olanow, M. C. Rodriguez-Oroz, P. Crack, and R. Kumar, "Deep-Brain Stimulation of the Subthalamic Nucleus or the Pars Interna of the Globus Pallidus in Parkinson's Disease", N. Engl. J. Med., vol. 345, no. 13, 2001, pp. 956-963.

[2] N. Suthana et al., "Memory enhancement and deep-brain stimulation of the entorhinal area", N. Engl. J. Med., vol. 366, 2012, pp. 502-510.

[3] C. Hamani, S. S. Stone, A. Garten, A. M. Lozano, and G. Winocur, "Memory rescue and enhanced neurogenesis following electrical stimulation of the anterior thalamus in rats treated with corticosterone", Exp. Neurol., vol. 232, no. 1, 2011, pp. 100-104.

[4] R. Gross and A. M. Lozano, "Advances in neurostimulation for movement disorders", Neurol Res., vol. 22, 2000, pp. 247-258.

[5] J. Kuhn et al., "Deep Brain Stimulation in Schizophrenia", Fortschritte der Neurol. Psychiatr., vol. 79, 2011, pp. 632-641.

[6] V. Vandewallea, C. van der Lindena, H. J. Groenewegena, and J. Caemaert, "Stereotactic treatment of Gilles de la Tourette syndrome by high frequency stimulation of thalamus", Lancet, vol. 353, no. 9154, 1999, p. 724.

[7] G. Deuschl et al., "Stimulation of the subthalamic nucleus at an earlier disease stage of Parkinson's disease: concept and standards of the EARLYSTIM-study", Parkinsonism Relat. Disord., vol. 19, no. 1, Jan. 2013, pp. 56-61.

[8] J. L. Alberts et al., "Bilateral subthalamic stimulation impairs cognitive-motor performance in Parkinson's disease patients", Brain, vol. 131, no. Pt 12, Dec. 2008, pp. 3348-60.

[9] A. Chaturvedi, C. R. Butson, S. Lempka, S. E. Cooper, and C. C. McIntyre, "Patient-specific models of deep brain stimulation: influence of field model complexity on neural activation predictions", Brain Stimul., vol. 3, no. 2, 2010, pp. 65-7.

[10] H. C. Martens et al., "Spatial steering of deep brain stimulation volumes using a novel lead design", Clin. Neurophysiol., vol. 122, no. 3, Mar. 2011, pp. 558-66.

[11] M. Åström, J. Lemaire, and K. Wårdell, "Influence of heterogeneous and anisotropic tissue conductivity on electric field distribution in deep brain stimulation", Med. Biol. Eng. Comput., vol. 50, no. 1, 2012, pp. 23-32.

[12] D. Andreuccetti, R. Fossi, and C. Petrucci, "Dielectric properties of body tissue", 2005. Available: http://niremf.ifac.cnr.it/tissprop/ [accessed: 2015-05-04].

[13] W. M. Grill, J. T. Mortimer, "Electrical properties of implant encapsulation tissue", Ann. Biomed. Eng., vol. 22, no. 1, 1994, pp. 23-33.

[14] D. R. McNeal, "Analysis of a model for excitation of myelinated nerve", IEEE Trans. Biomed. Eng., vol. 23, no. 4, Jul. 1976, pp. 329-337.

[15] F. Rattay, "Analysis of models for external stimulation of axons", IEEE Trans. Biomed. Eng., vol. 33, 1986, pp. 974-977.

[16] M. Åström, E. Diczfalusy, H. C. Martens, and K. Wårdell, "Relationship between Neural Activation and Electric Field Distribution during Deep Brain Stimulation", IEEE Trans. Biomed. Eng., vol. 62, no. 2, 2015, pp. 664-672.

[17] R. Cubo, M. Åström, and A. Medvedev, "Target coverage and selectivity in field steering brain stimulation", 36th Annual International Conference of the IEEE EMBS, Chicago, IL, 2014, pp. 522-525.

[18] J. D'Errico. Inhull function. MATLAB File Exchange. URL: http://mathworks.com/matlabcentral/fileexchange/10226-inhull [accessed: 2015-05-04].

[19] R. Cubo, M. Åström, and A. Medvedev, Stimulation field coverage and target structure selectivity in field steering brain stimulation, Mov. Disord., vol. 29, no. S1, pp. S198-S199, 2014.

[20] S. F. Lempka, M. Johnson, S. Miocinovic, J. L. Vitek, and C. C. McIntyre, "Current-controlled deep brain stimulation reduces in vivo voltage fluctuations observed during voltage-controlled stimulation", Clin. Neurophysiol., vol. 121, no. 12, 2010, pp. 2128-2133.